



HAL
open science

Interactive segmentation: a scalable superpixel-based method

Bérengère Mathieu, Alain Crouzil, Jean-Baptiste Puel

► **To cite this version:**

Bérengère Mathieu, Alain Crouzil, Jean-Baptiste Puel. Interactive segmentation: a scalable superpixel-based method. Journal of Electronic Imaging, 2017, 26 (6), pp.1-18. 10.1117/1.JEI.26.6.061606 . hal-03512910

HAL Id: hal-03512910

<https://hal.science/hal-03512910>

Submitted on 5 Jan 2022

HAL is a multi-disciplinary open access archive for the deposit and dissemination of scientific research documents, whether they are published or not. The documents may come from teaching and research institutions in France or abroad, or from public or private research centers.

L'archive ouverte pluridisciplinaire **HAL**, est destinée au dépôt et à la diffusion de documents scientifiques de niveau recherche, publiés ou non, émanant des établissements d'enseignement et de recherche français ou étrangers, des laboratoires publics ou privés.



Open Archive Toulouse Archive Ouverte

OATAO is an open access repository that collects the work of Toulouse researchers and makes it freely available over the web where possible

This is an author's version published in:
<http://oatao.univ-toulouse.fr/19167>

Official URL

DOI : <https://doi.org/10.1117/1.JEI.26.6.061606>

To cite this version: Mathieu, Bérengère and Crouzil, Alain and Puel, Jean-Baptiste *Interactive segmentation: a scalable superpixel-based method.* (2017) *Journal of Electronic Imaging*, 26 (6). 1-18.
ISSN 1017-9909

Any correspondence concerning this service should be sent to the repository administrator: tech-oatao@listes-diff.inp-toulouse.fr

Interactive segmentation: a scalable superpixel-based method

Béregère Mathieu,^a Alain Crouzil,^{a,*} and Jean-Baptiste Puel^b

^aUniversité Toulouse III, Institut de Recherche en Informatique de Toulouse, Toulouse, France

^bUniversité Toulouse III, Ecole Nationale Supérieure de Formation de l'Enseignement Agricole, Toulouse, France

Abstract. This paper addresses the problem of interactive multiclass segmentation of images. We propose a fast and efficient new interactive segmentation method called superpixel α fusion (S α F). From a few strokes drawn by a user over an image, this method extracts relevant semantic objects. To get a fast calculation and an accurate segmentation, S α F uses superpixel oversegmentation and support vector machine classification. We compare S α F with competing algorithms by evaluating its performances on reference benchmarks. We also suggest four new datasets to evaluate the scalability of interactive segmentation methods, using images from some thousand to several million pixels. We conclude with two applications of S α F.

DOI: [10.1117/1.JEI.26.6.061606](https://doi.org/10.1117/1.JEI.26.6.061606)

Keywords: image analysis; interactive segmentation; superpixel; graph-factor; support vector machine; dataset; image editing

1 Introduction

Image segmentation is still a challenging research topic in the image analysis community. Its goal is to group similar and neighboring pixels in order to partition the image into structures corresponding to coherent elements. However, depending on the application context, even for the same image, the term “coherent elements” can have different meanings. An example is given in Fig. 1, which shows for the same image two possible segmentations. In the first case, we want to select only the main character, for example, to copy and paste it on another background. In the second case, we are interested in some details, like the clothing.

This example illustrates the complexity of finding a segmentation algorithm able to deal with the variety of contexts of use. During the last decade, convolutional neural networks (CNNs) had led to significant advances in the semantic segmentation task.^{1–3} However, even if results of CNN methods are impressive, it is not yet possible to correct errors of the produced segmentation and, to the best of our knowledge, the user input can be used⁴ only during the training stage. Even if the output of a CNN can be used as the input of an optimization process constrained by the user input, it requires an extensive dataset for training. Currently, we think that there is always room for interactive methods with an iterative process allowing the user to correct errors of the method and to achieve any desired segmentation. For each image, according to his needs, the user can change the object categories and the level of details. Basically, the user chooses some pixels (named seeds) and indicates for each of them the element to which it belongs. Additional constraints about the wanted segmentation are deduced by analyzing these seeds. Adding or removing some seeds can improve the produced result.

The two most common application scopes for these kinds of algorithms are segmentation of a particular anatomic

structure in medical imagery^{5–14} and natural photograph (such as an image taken with a smartphone or a camera) manipulation for art or graphic design purpose.^{15–26} These two application scopes correspond to distinct problems, with substantial differences among proceeded image features and the available prior information. Thus, in the scope of this paper, we focus only on interactive segmentation to select one or several objects in natural photographs.

1.1 Previous Work

Currently, several interactive segmentation methods solve only binarization problems by separating a desired foreground object from the background. These methods may be boundary-based^{21–23} or region-based.^{15–20,24–28} Figure 2 shows the most common way to give seeds, related to each category.

In boundary-based methods, the user provides landmark points and the algorithm links them with a closed curve, which satisfies both regularization and edge evidence constraints. The combination of piecewise-geodesic paths (CPP) is one of the most recent boundary-based interactive segmentation methods. Proposed by Mille et al.,²¹ this algorithm generates several relevant paths and selects the one minimizing an energy function that decreases when the path has a high probability to be on an image edge, when the regions inside and outside the path are homogeneous and when the path contains few self-overlaps and self-intersections.

In region-based methods, the user gives seeds by drawing strokes on the objects. Pixels are grouped to form regions, according to the similarity to object models created by the seeds. The interactive graph cuts (IGC) algorithm, proposed by Boykov and Jolly,¹⁶ operates by minimizing an energy function E grouping hard constraints (seeds provided by user interaction) and soft constraints (similarities between pixels in spatial and intensity domains). To find the

*Address all correspondence to: Alain Crouzil, E-mail: alain.crouzil@irit.fr

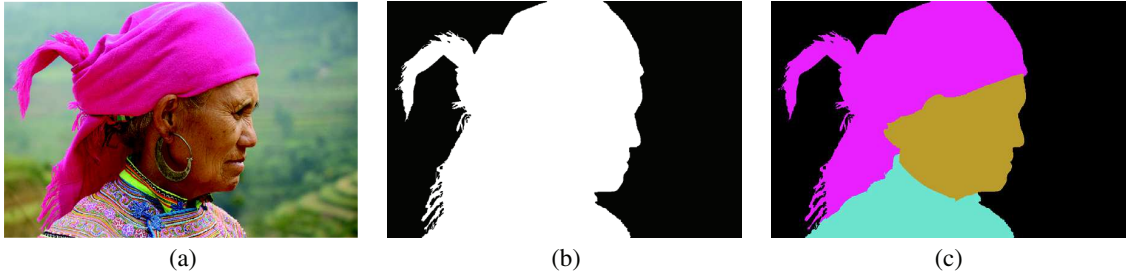


Fig. 1 Two segmentation results of the same image. (a) Original image, (b) a coarse segmentation, and (c) a finer segmentation.

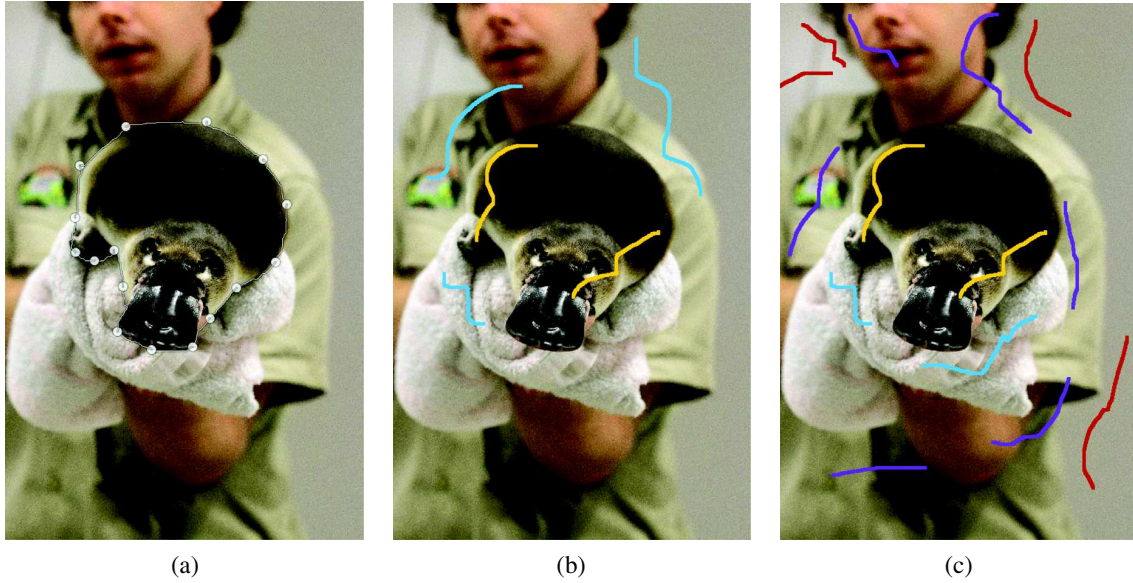


Fig. 2 User interaction for the different categories of interactive segmentation methods. (a) Boundary-based, (b) region-based, and (c) region-based multiclass interactive binarizations.

segmentation S^* , which minimizes E , Boykov and Jolly¹⁶ used a fast min-cut/max-flow algorithm on the graph $G = \langle V, E \rangle$ with:

- $V = V_p \cup V_r$, where:
 - $V_p = \{v_1, \dots, v_n\}$ is a set of nodes such that each pixel p_i is linked to a node v_i ;
 - $V_r = \{T, S\}$ is a set grouping two particular nodes: the sink T and the source S ;
- $E = E_p \cup E_r$, where:
 - E_p is the set of edges linking V_p nodes, under a standard 4- or 8-neighborhood system;
 - E_r is the set of edges linking each node in V_p to each node in V_r .

Each edge is weighted such that E_p edges have a strong weight if the two linked nodes correspond to similar pixels and E_r edges have a high weight if the V_p node has a strong probability to belong to the foreground when the second node is the source and to the background when the second

node is the sink. The method of Boykov and Jolly¹⁶ obtained very good results in the McGuinness interactive segmentation review,²⁹ but it solves only a binary classification problem.

In the McGuinness et al. review,²⁹ the interactive segmentation method using binary partition trees (BPT) of Salembier et al.²⁵ is the main challenger of IGC. Starting from a hierarchical segmentation of the image represented as a BPT, the algorithm produces a binarization by merging regions. First, according to the seeds given by the user, some leaf nodes of the binary tree are labeled. Then, these labels are propagated to the parent nodes, until a conflict occurs when the two children of a node have different labels. In this situation, the parent node is marked as conflicting. Finally, all nonconflicting nodes propagate their labels to their children. At the end of this stage, some subtrees can remain unlabeled. These unclassified regions are labeled with the label of a previously classified adjacent region. When several adjacent regions with different labels are candidates to label the unclassified region, the closest one according to the Euclidean distance is chosen.

The simple interactive object extraction proposed by Friedland et al.¹⁷ uses seeds to generate color signatures³⁰

of background and foreground, represented as a weighted set of cluster centers. The distances between each remaining pixel and any of these centers are computed. The pixels are merged with the region including the closest cluster.

To the best of our knowledge, the last proposition of an interactive region-based binarization method is the segmentation algorithm of Jian et al.³¹ using adaptive constraint propagation (ACP). First, the image is segmented using the mean-shift method. Then, features of corresponding regions are extracted. During the following step of ACP, pairwise constraints are generated by analyzing the given seeds. Next, ACP is performed in order to learn a global discriminative structure of the image. This structure allows finally assigning each region to the background or the foreground.

The seeded region growing (SRG) algorithm, proposed by Adams et al.,¹⁵ the interactive multilabel segmentation (IMS) method of Santner et al.,²⁶ the robust IMS with an advanced edge detector (RIMSAED) of Müller et al.,²⁸ and the robust interactive image segmentation (RIIS) of Oh et al.³² are attempts to solve the multiclass interactive segmentation problem.

The method of Adams and Bischof¹⁵ is a very simple recursive method, where regions are characterized by their average color. The initial regions begin with the pixels labeled by the user. Then, the regions are grown by including the adjacent pixels with the most similar color. The average colors are updated and the algorithm iterates until all the pixels have been grouped. In spite of its speed, this algorithm suffers from the simplicity of its region color model.

The IMS algorithm²⁶ has two major steps. First, the pixel likelihood to belong to each class is computed thanks to a random forest (RF) classifier. Then, an optimal segmentation is found by minimizing an energy function that linearly combines a regularization term and a data term

$$E = \frac{1}{2} \sum_{i=1}^N \text{Per}_D(E_i; \Omega) + \lambda \sum_{i=1}^N \int_{E_i} f_i(x) dx, \quad (1)$$

where Ω is the image domain, E_i are the N pairwise disjoint sets partitioning Ω , Per_D is a function encouraging to have smooth boundaries following pixels with high gradient value, and f_i is the output of the RF classifier. During the first stage, color and texture descriptors of pixels are computed. Santner et al.²⁶ compared several features and showed that the combination of Lab color space and local binary pattern texture descriptor gives the best results. Next, the classifier is trained with the seeds. The trained classifier gives for each pixel the likelihood to belong to each class. These likelihoods are used during the second step, into the data term. The regularization term penalizes the boundary length, avoiding noisy segmentation. Santner et al.²⁶ formulated the segmentation problem like a Potts model and solve it using a first-order primal-dual algorithm. However, this method is rather slow. Santner et al.²⁶ proposed a massive parallelization and a GPU implementation of IMS, segmenting an image of 625×391 pixels into four classes on a desktop PC featuring a 2.6-GHz quad-core processor in about 2 s.

The RIMSAED method of Müller et al.,²⁸ similarly to IMS method, minimizes Eq. (1). Nevertheless, in the RIMSAED algorithm, the term Per_D does not simply use gradient magnitude but a more accurate edge detector,³³ which incorporates texture, color, and brightness. The data

term depending on f_i uses color and location distributions of seeds to deduce the likelihood of a pixel to belong to each class. This approach is similar to the one used by Nieuwenhuis and Cremers.³⁴ The contribution of Müller consists of using potential functions that allow the segmentation method to correct wrong seeds by introducing a prior probability of seeds to be erroneous.

For their proposed method RIIS, Oh et al.³² used occurrence (capturing global distribution of all color values within seeds) and cooccurrence (encoding a local distribution of color values around seeds) probabilities to detect and exclude the erroneous seeds. Occurrence and cooccurrence probabilities are computed using a histogram of gray level values of seeds. They produce a confidence score for each seed. The final segmentation is obtained by minimizing an energy similar to the one used by Boykov and Jolly¹⁶. The energy function contains a data term that checks the homogeneity of resulting regions as well as the consistency with seeds. It also integrates a regularization term encouraging similar pixels to be merged. As RIIS has a regularization term adopting a nonlocal pairwise connection by computing k -nearest neighbors (k -NN) in the feature space, an approximation of the optimal solution is found using sparse solvers.³⁵

1.2 Contributions

The main contribution of this paper is an interactive multiclass segmentation method, named *SaF*. The *SaF* algorithm achieves results similar to or better than state-of-the-art methods, while keeping a low algorithmical complexity that allows it to correctly segment images having millions of pixels.

The computation of an accurate segmentation is ensured by formulating the interactive segmentation problem as a discrete energy minimization problem, given in the form of a factor graph.³⁶ Notably, we propose a regularization term that significantly reduces the required number of seeds while allowing the correct segmentation of small objects belonging to rare classes. The consistency of the segmentation result regarding the image visual features and the seeds given by the user is obtained by a supervised learning stage.

The efficiency and the scalability of *SaF* are ensured by an oversegmentation initialization step. Oversegmentation is the task of grouping pixels into small homogeneous regions, called superpixels. During the last decade, a lot of methods have been suggested and a recent review³⁷ shows that five of them achieve similar results. By providing a new evaluation benchmark of photographs of several million pixels, we point to unexpected difficulties encountered by these methods and justify the use of the simple linear iterative clustering (SLIC) algorithm in *SaF*.

We evaluate *SaF* with state-of-the-art benchmarks and we quantitatively analyze its scalability by creating and making available four new datasets with, respectively, big images (1800×1201 pixels), medium images (1350×901 pixels), small images (1013×675 pixels), and tiny images (500×334 pixels). We provide an implementation of *SaF* as a Gimp plugin and we use *SaF* in a landscape teaching Android application.

In the following sections, we will first explain the modeling of the interactive segmentation problem as a discrete optimization problem, represented by a factor graph. Then, we will describe experiments to choose components that

are now parts of SaF and how we configure those components. Finally, we will evaluate its performance by comparing it to the height of state-of-the-art methods, against three different benchmarks. We will conclude with two examples of applications.

2 Interactive Segmentation as a Discrete Optimization Problem

Let $X = \{x_1, \dots, x_M\}$ be a partition of an image I in M connected components. In the case of SaF algorithm, these connected components are small sets of similar pixels, called superpixels. Computing a multiclass segmentation of I means to assign to each superpixel x_i a label λ_j related to the class j . Usually, λ_i is a positive integer and for K classes, the set of labels that may be given for a region is $\Lambda = \{\lambda_1, \dots, \lambda_K\}$. In the case of interactive segmentation, K is deduced by analyzing the number of colors used by the user when drawing the seeds.

Let $G = \langle X, E \rangle$ be an undirected graph, where X is the set of vertices (one vertex by superpixel) and E is the set of edges, linking each pair of superpixels containing adjacent pixels. Let $c = \{c_1, \dots, c_N\}$ be a set of random variables, indexed by the vertices of G , such that $c_i \in \Lambda$. We assume that G is a Markov random field (MRF). Thus, we can find an optimal segmentation c^* of the image I by minimizing

$$E_{\text{MRF}}(c|I) = \exp \left[\sum_{i=1}^N f^{\text{data}}(x_i, c_i) + \sum_{(x_i, x_j) \in E} \omega(x_i) f^{\text{reg}}(x_i, c_i, x_j, c_j) \right], \quad (2)$$

where f^{data} is a data term, f^{reg} is a regularization term, and ω is a weighting function. The following optimization problem can be easily modeled by a factor graph, which represents the structure of the underlying problem in a more precise and explicit way than MRF can.³⁸

A factor graph $G' = \langle X', F', E' \rangle$ is a bipartite graph representing the factorization of a function of M variables, $g(x_1, \dots, x_M)$, by

- X' a set of vertices denoting the M variables;
- F' a set of vertices related to the decomposition of g in subfunctions called factors;
- E' is the set of edges linking each factor to its related variables.

Figure 3 shows the concept of factor graph.

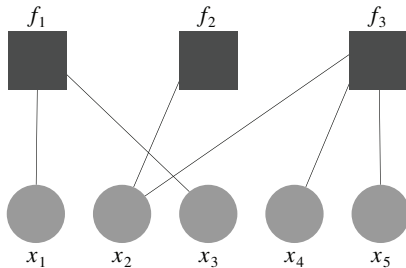


Fig. 3 Factor graph modeling the factorization: $F_1(X_1, X_2, X_3, X_4, X_5) = f_1(X_1, X_3) f_2(X_2) f_3(X_2, X_4, X_5)$.

In the case of Eq. (2), the factorization is straightforward

$$E_{\text{FG}} = \prod_{i=1}^N \mathfrak{F}^{\text{data}}(x_i, c_i) \prod_{(x_i, x_j) \in E} \mathfrak{F}^{\text{reg}}(x_i, c_i, x_j, c_j), \quad (3)$$

where $\mathfrak{F}^{\text{data}}(x_i, c_i) = \exp[f^{\text{data}}(x_i, c_i)]$ and $\mathfrak{F}^{\text{reg}}(x_i, c_i, x_j, c_j) = \exp[\omega(x_i) f^{\text{reg}}(x_i, c_i, x_j, c_j)]$.

2.1 Data Term

Let $X = \langle X_G, X_C \rangle$ be a partition of X into two sets: X_G for the superpixels containing seeds of only one class and X_C for the superpixels that do not contain seeds or contain seeds of several classes. The set X_G allows computing the probability $p(\lambda_j|x_i)$ for the superpixel x_i to belong to the class of label λ_j . As we want to minimize Eq. (3), the data term is given by

$$f^{\text{data}}(x_i, c_i) = 1 - p(\lambda_j|x_i), \quad \text{where } c_i = \lambda_j. \quad (4)$$

For multiclass classification problems, the second approach of Wu et al.³⁹ is well known to give a satisfactory approximation of the probability of a variable to belong to a given class, using the result of a supervised learning method. This algorithm has been tested both with a support vector machine (SVM) and a RF. Section 3.3 explains how we empirically chose one of them to compute the data term.

2.2 Regularization Term

The segmentation result obtained from the minimization of f^{data} could be very noisy, with isolated superpixels having a label different from its neighbors. On one hand, removing this noise by adding seeds is a tedious task and degrades the user experience. On the other hand, a regularization term encouraging large and compact regions can remove rare classes corresponding to small objects.

In this paper, we propose a regularization term f^{reg} , designed to increase spatial consistency of given labels while preserving rare classes. In a segmentation result, let x_n be a noisy superpixel (i.e., a superpixel with an erroneous label) and x_r a superpixel of a rare class. Both x_n and x_r have a majority of neighbors with different labels. Let λ_n be the label of x_n and λ_r the label of x_r . The fact that a superpixel has the label λ_r and several adjacent superpixels with labels different from λ_r is more common than the fact that a superpixel has the label λ_n and several neighbors with labels different from λ_n . Figure 4 shows an example where superpixels in blue (the rare class) are more likely adjacent to superpixels in black than to superpixels in pink. In other words, the probability for a superpixel in blue to have neighbors in black is higher than the probability for a superpixel in pink to have neighbors in black. By estimating these two probabilities, we can distinguish between correctly labeled superpixels belonging to rare classes and noise.

The steps for the computation of the regularization term are the following. First, SaF produces a preliminary segmentation, by assigning to each superpixel the most likely label, according to the result given by the supervised learning method used in the data term estimation. This segmentation is analyzed to compute for each class i , $p_i(j)$ is the probability for a superpixel of class i to have a neighbor of class j , where $j \in [1, K]$.

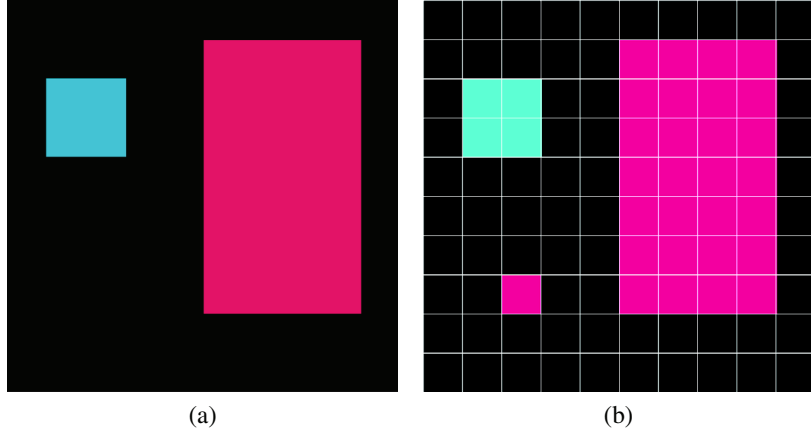


Fig. 4 Problem of the distinction between rare classes and noise in segmentation. (a) Image with three classes, two dominant classes (in black and pink), and one rare class (in blue). (b) Example of a noisy segmentation. Boundaries of superpixels are in white.

The regularization term is finally given by

$$f^{\text{reg}}(x_i, c_i, x_j, c_j) = 1 - \max[p_i(j), p_j(i)]. \quad (5)$$

2.3 Weighting Function

Weighting function ω allows balancing the influence of the regularization term with respect to the data term. Unlike pixels, superpixels have varying numbers of neighbors. The influence of the regularization term depends on this number and the weighting function should include it. After several tests on a subset of state-of-the-art benchmarks (see Sec. 4), we empirically choose the following weighting function:

$$\omega(x_i) = \frac{0.7}{|\text{nei}(x_i)|}, \quad (6)$$

where $|\text{nei}(x_i)|$ is the number of neighbors of superpixel x_i .

2.4 Inference Method

Due to the number of possible segmentations, the search of the one minimizing Eq. (3) is not realistically feasible. Following the conclusions of Kappes et al.³⁶ for image analysis problems with superpixels, we use a generalization of the α expansion algorithm of Boykov et al.,⁴⁰ the α fusion algorithm, with the fusion-moves and the order-reduction of Fix et al.⁴¹

2.5 Algorithm Overview

Figure 5 shows an overview of the proposed SaF algorithm, which can be divided into an initialization stage extracting image features and a segmentation stage taking seeds into account.

We consider an image I that must be segmented. During the initialization step, SaF groups pixels of I into N superpixels. As explained above, superpixels are small homogeneous color regions, significantly less numerous than pixels. Thus, using them as visual primitives instead of pixels significantly reduces the execution times of the next algorithm steps. In the context of SaF algorithm, superpixels

are used as an image compression tool. Their features are extracted to produce a set P^* of N vectors.

The segmentation stage of SaF is iterative: as long as the user adds or removes seeds, the segmentation is updated. We start by analyzing seeds provided by the user to deduce K , the number of classes. We create a set of $K + 1$ labels $\{0, 1, \dots, K\}$ with $1, \dots, K$ the labels representing each class and 0 a void label. So, we can assign to each pixel p a label j such that $j > 0$ if p is a seed or $j = 0$ otherwise. Then, for each class, we create S_j , the set of superpixels including at least one pixel with label j and the others with label j or 0. Next, we train a classifier for multiclass classification, using, for each class j , the features of the superpixel set S_j . Finally, we compute data and regularization terms as explained in Sec. 2 and we use α fusion algorithm to find an optimal labeling of the superpixels. The label given to each superpixel is assigned to each pixel belonging to it, producing the segmentation.

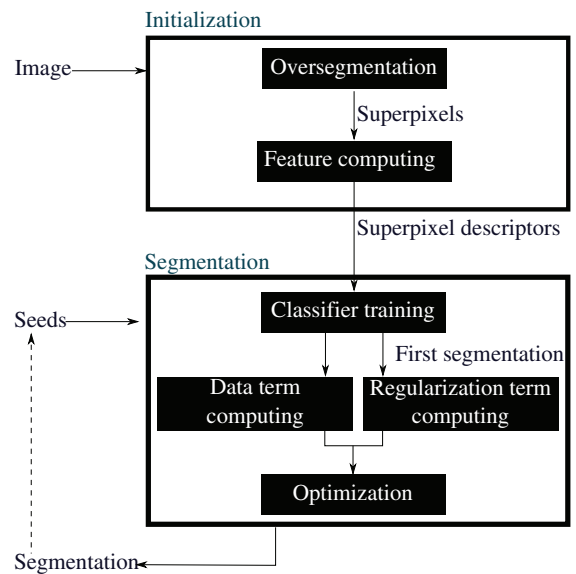


Fig. 5 SaF algorithm overview.

3 Experiments to Select and Tune SaF Components

3.1 Oversegmentation

Superpixels are the results of an oversegmentation of the image: boundaries of objects in the image should match superpixel boundaries, but the same object can be partitioned into several superpixels. In the context of interactive segmentation, a good oversegmentation algorithm must produce as few superpixels as possible and make as few object overlapping errors as possible, because they cannot be corrected by the next steps of the algorithms. Unfortunately, reducing the number of superpixels requires increasing their size and, by grouping more and more pixels into a same superpixel, the probability of errors increases dramatically. Moreover, the superpixel extraction has to be fast, avoiding that this preprocessing step slows down the whole method.

According to the Stutz review,³⁷ Felzenszwalb algorithm (FZ),⁴² quick shift (QS),⁴³ entropy rate superpixels (ERS),⁴⁴ SLIC,⁴⁵ and contour relaxed superpixels (CRS)⁴⁶ outperform other oversegmentation algorithms. In addition, all these methods achieve similar results in both precision and execution time. However, the datasets used by Stutz contain only small images (some thousand pixels). To check that these algorithms remain competitive when dealing with big images (several million pixels), we provide a heterogeneous size image dataset (HSID), containing 100 images and the corresponding ground truth.

We evaluated FZ, QS, ERS, SLIC, and CRS as well as the two most recent oversegmentation methods: algorithm of Rubio et al. [boundary-aware superpixel segmentation (BASS)]⁴⁷ and waterpixel (WP)⁴⁸ algorithm. We use implementations made available by their authors.

To quantify superpixel boundary adherence, we adapt the common boundary recall measure, using fuzzy-set theory to introduce some tolerance error near the border pixels

$$\text{FBR}(S, G) = \frac{1}{|B_G|} \sum_{p \in B_G} \exp \left[-\frac{d(p - p')^2}{2\sigma^2} \right], \quad (7)$$

where G is a ground truth, S is the oversegmentation result, B_G is the set of boundary pixels in G , B_S is the set of boundary pixels in S , $d(p - p')$ is the distance between p and p' , the nearest boundary pixel in S , $p' = \arg \min_{p_j \in B_S} [d(p - p_j)]$.

The bandwidth parameter σ regulates the sensitivity to the error by penalizing more or less the pixels far from the boundary. According to McGuinness et al.,²⁹ we set it to 4.

We made seven tests where methods are configured to, respectively, produce about 500 (test 1), 700 (test 2), 900 (test 3), 1100 (test 4), 1300 (test 5), 1500 (test 6), and 1700 (test 7) superpixels (Figs. 6 and 7).

Figure 6 shows the evolution of FBR scores with respect to the number of superpixels. The evolution of the execution time is given in Fig. 7.

Results show that QS, BASS, CRS, and WP fail to correctly oversegment HSID images. Algorithms FZ, SLIC, and ERS achieve similar boundary adherence with an equivalent number of superpixels, but ERS and FZ are significantly slower than SLIC. As the execution time is critical for an interactive segmentation method, we chose to use SLIC.

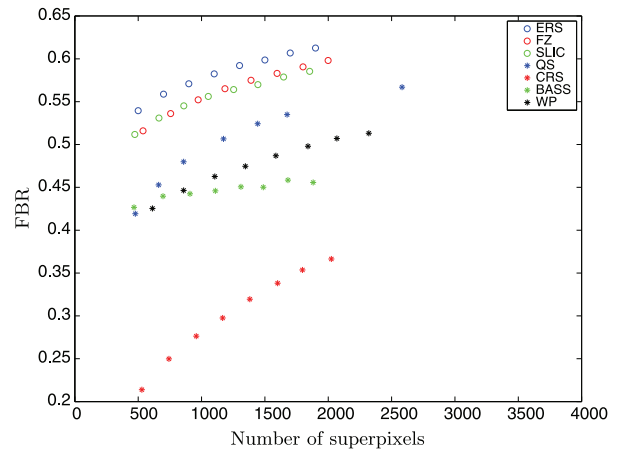


Fig. 6 Boundary adherence evolution (FBR) with respect to the number of superpixels.

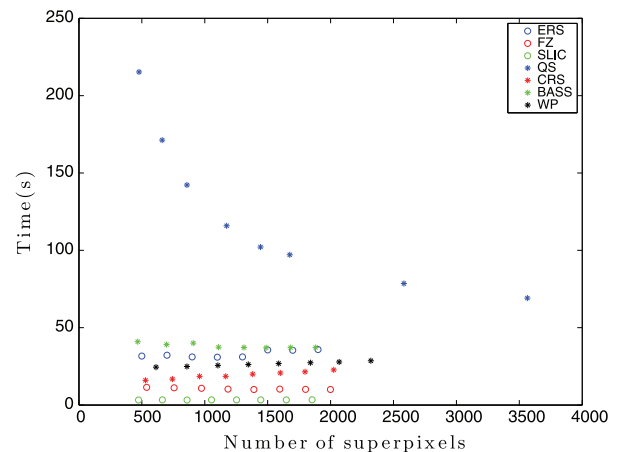


Fig. 7 Execution time evolution with respect to the number of superpixels.

The HSID dataset and the complete results of the evaluation are available at Ref. 49. They are described in a previous paper.⁵⁰

3.2 Descriptor

We describe each superpixel by its normalized average RGB color and the normalized location of its center of mass. We made additional tests with Lab color space and obtained results similar to those achieved with RGB. As converting a pixel from RGB to Lab color spaces requires extra computation, we chose to use only RGB color space.

This simple descriptor has the benefit of being quickly computed and used. In addition, as explained in Sec. 4.4, color and location are intuitive concepts for the user and make the behavior of SaF easily predictable.

However, some previous works (for example, the method of Gould et al.⁵¹) show that texture information from superpixels is often also valuable. Thus, we designed another version of SaF with color, location, and texture features. As a texture descriptor, we used uniform local binary patterns (LBP-U),⁵² which have been successfully integrated

in many applications.²⁶ We evaluated it with the seven datasets and their related metrics presented in Sec. 4. While the computation of LBP-U represents only 23% of the total execution time of the initialization stage, the impact of the addition of a texture descriptor in the segmentation stage is more significant, taking 76% of the total execution time. The segmentation stage occurs each time the user updates the seeds, and this result led us to discard the LBP-U version of SaF.

Moreover, on all the tested datasets, we did not find any evidence that LBP-U information can improve accuracy or allow reducing the number of required seeds. Because in SaF the SLIC oversegmentation algorithm is tuned to produce very small regions (about a few hundred of pixels) with homogeneous colors (average standard deviation for each color channel is about 4%), this result is not surprising.

3.3 Classifier

We evaluated the accuracy of probability distribution predicted by two different classifiers integrated in the approach of Wu et al.: an RF and an SVM. For RF, we used the ALGLIB implementation.⁵³ Two parameters, the number of decision trees and the percentage of training data used to train each decision tree, must be given. For the SVM, we used the C-SVM libSVM implementation⁵⁴ with a radial basis function kernel. With this kind of kernel, two parameters, the regularization parameter C and the kernel parameter γ , must be tuned. We tested each classifier with different pairs of parameters, on a subset of Santner dataset,²⁶ to analyze how its behavior evolves when parameters are modified.

We used the multiclass segmentation evaluation dataset D_{SA} ⁵⁵ made available by Santner et al.²⁶ As we reuse this dataset to compare SaF to the state-of-the-art methods, we use only a subset of these ground truth, made of 100 images.

Using this dataset, we estimate reference distribution probabilities for each superpixel of each image. We compute for each class λ_j the ratio of pixels belonging to superpixel x_i and having label λ_j in the ground truth.

We used two criteria: the average execution time for an image and the distance between the reference probability distribution and the one predicted using the classifier and the approach of Wu et al.³⁹ Execution time is calculated on a desktop PC featuring a 2.6-GHz Intel Core i7 processor. The similarity between the two probability distributions is computed using

$$\mathfrak{F}_{\text{err}}(P_R, P_{\text{classif}}) = \sum_{i=1}^{N_\lambda} \sqrt{[p_{\text{classif}}(\lambda_i|x_i) - p_{gt}(\lambda_i|x_i)]^2}, \quad (8)$$

where $p_{\text{classif}}(\lambda_i|x_i)$ is the probability of superpixel x_i to belong to the class of label λ_i predicted by a classifier and $p_{gt}(\lambda_i|x_i)$ is the related reference probability.

To train classifiers, we use randomly selected superpixels. The same training data are used for the both RF and SVM. The results presented in Tables 1–4 are obtained by using about one hundred superpixels as training data. We made additional tests by increasing or decreasing the number of training data. Tendencies remain the same.

Tables 1 and 2 show that, for SaF with RF, a low $\mathfrak{F}_{\text{err}}$ score is achieved with a high number of decision trees and using a substantial percentage of training data for each

Table 1 Execution time (in a tenth of a second) of RF classifier, achieved on a subset of the ground truth of Santner et al.²⁶ The first row gives the percentage of training data per tree, the first column gives the number of trees.

| | 10 | 20 | 30 | 40 | 50 | 60 | 70 | 80 | 90 | 100 |
|------|-----|-----|-----|-----|------|------|------|------|------|------|
| 100 | 0.8 | 1.6 | 2.6 | 3.3 | 4.1 | 4.9 | 5.7 | 6.6 | 7.4 | 8 |
| 200 | 1.1 | 2.1 | 3.2 | 4.4 | 5.5 | 6.4 | 7.5 | 8.6 | 9.8 | 10.5 |
| 300 | 1.3 | 2.5 | 3.8 | 5.1 | 6.5 | 7.7 | 9 | 10.3 | 11.8 | 12.7 |
| 400 | 1.4 | 2.9 | 4.4 | 6 | 7.3 | 8.8 | 10.8 | 11.9 | 13.5 | 15.2 |
| 500 | 1.6 | 3.2 | 5 | 6.6 | 8.3 | 10 | 11.6 | 13.4 | 15.4 | 16.9 |
| 600 | 1.7 | 3.5 | 5.6 | 7.5 | 9.3 | 11.1 | 12.9 | 14.8 | 17 | 18.5 |
| 700 | 1.9 | 3.8 | 6.5 | 8.1 | 10 | 11.9 | 14.1 | 16.2 | 18 | 19.6 |
| 800 | 2.1 | 4.2 | 6.8 | 8.8 | 10.8 | 12.9 | 15.9 | 17.9 | 19.1 | 21.3 |
| 900 | 2.2 | 4.5 | 7.3 | 9.4 | 11.7 | 14.1 | 17 | 19.1 | 20.5 | 22.9 |
| 1000 | 2.4 | 5 | 7.6 | 9.9 | 12.8 | 14.9 | 18 | 20.6 | 22 | 24.6 |

Table 2 Error rate $\mathfrak{F}_{\text{err}}$ (%) of RF classifier, achieved on a subset of the ground truth of Santner et al.²⁶ The first row gives the percentage of training data per tree, the first column gives the number of trees.

| | 10 | 20 | 30 | 40 | 50 | 60 | 70 | 80 | 90 | 100 |
|------|----|----|----|----|----|----|----|----|----|-----|
| 100 | 13 | 13 | 13 | 13 | 13 | 13 | 13 | 13 | 13 | 13 |
| 200 | 10 | 9 | 9 | 10 | 9 | 10 | 10 | 9 | 9 | 9 |
| 300 | 8 | 8 | 8 | 8 | 8 | 8 | 8 | 8 | 8 | 8 |
| 400 | 7 | 7 | 7 | 7 | 7 | 7 | 7 | 7 | 7 | 7 |
| 500 | 6 | 6 | 6 | 6 | 6 | 6 | 6 | 6 | 6 | 6 |
| 600 | 6 | 6 | 6 | 6 | 6 | 6 | 6 | 6 | 6 | 6 |
| 700 | 5 | 5 | 5 | 5 | 5 | 5 | 5 | 5 | 5 | 5 |
| 800 | 5 | 5 | 5 | 5 | 5 | 5 | 5 | 5 | 5 | 5 |
| 900 | 5 | 5 | 5 | 5 | 5 | 5 | 5 | 5 | 5 | 5 |
| 1000 | 5 | 5 | 5 | 5 | 5 | 5 | 5 | 5 | 5 | 5 |

decision tree, which comes at the cost of a significantly increased execution time.

On the contrary, Tables 3 and 4 show that there are some pairs of values for parameters γ and C giving both a low $\mathfrak{F}_{\text{err}}$ score and a fast classification, for example, $\gamma = 4$ and $C = 4$, $\gamma = 4$ and $C = 8$, $\gamma = 8$, $C = 8$, etc.

We explain the difference between the two classifiers by the fact that SVM uses the whole training data, whereas RF trains each decision tree with a subset of the training data. In interactive segmentation problems, the low number of training data (especially when dealing with superpixels,

Table 3 Execution time (in a tenth of a second) of SVM classifier, achieved on a subset of the ground truth of Santner et al.²⁶ The first row gives the value of C parameter, the first column gives the value of parameter γ .

| | 2^{-6} | 2^{-5} | 2^{-4} | 2^{-3} | 2^{-2} | 2^{-1} | 1 | 2 | 2^2 | 2^3 | 2^4 | 2^5 | 2^6 | 2^7 | 2^8 | 2^9 |
|----------|----------|----------|----------|----------|----------|----------|-----|-----|-------|-------|-------|-------|-------|-------|-------|-------|
| 2^{-6} | 1 | 0.9 | 1 | 0.9 | 0.9 | 0.9 | 0.9 | 0.8 | 0.7 | 0.6 | 0.5 | 0.5 | 0.4 | 0.4 | 0.4 | 0.4 |
| 2^{-5} | 0.9 | 0.9 | 0.9 | 0.9 | 0.9 | 0.9 | 0.8 | 0.7 | 0.6 | 0.5 | 0.5 | 0.4 | 0.4 | 0.4 | 0.4 | 0.5 |
| 2^{-4} | 0.9 | 0.9 | 0.9 | 0.9 | 0.9 | 0.8 | 0.7 | 0.6 | 0.5 | 0.5 | 0.4 | 0.4 | 0.4 | 0.4 | 0.4 | 0.5 |
| 2^{-3} | 0.9 | 0.9 | 0.9 | 0.9 | 0.8 | 0.7 | 0.6 | 0.5 | 0.5 | 0.4 | 0.4 | 0.4 | 0.4 | 0.4 | 0.5 | 0.5 |
| 2^{-2} | 0.9 | 0.9 | 0.9 | 0.8 | 0.7 | 0.6 | 0.5 | 0.5 | 0.4 | 0.4 | 0.4 | 0.3 | 0.4 | 0.4 | 0.4 | 0.5 |
| 2^{-1} | 0.9 | 0.9 | 0.8 | 0.7 | 0.6 | 0.5 | 0.5 | 0.4 | 0.4 | 0.3 | 0.3 | 0.3 | 0.3 | 0.4 | 0.4 | 0.5 |
| 1 | 0.9 | 0.9 | 0.7 | 0.6 | 0.5 | 0.5 | 0.4 | 0.4 | 0.3 | 0.3 | 0.3 | 0.3 | 0.3 | 0.4 | 0.4 | 0.5 |
| 2 | 0.9 | 0.8 | 0.7 | 0.6 | 0.5 | 0.4 | 0.4 | 0.3 | 0.3 | 0.3 | 0.3 | 0.3 | 0.3 | 0.4 | 0.4 | 0.5 |
| 2^2 | 0.9 | 0.8 | 0.7 | 0.6 | 0.5 | 0.4 | 0.3 | 0.3 | 0.3 | 0.3 | 0.3 | 0.3 | 0.3 | 0.4 | 0.4 | 0.4 |
| 2^3 | 0.9 | 0.9 | 0.7 | 0.6 | 0.5 | 0.4 | 0.4 | 0.4 | 0.4 | 0.4 | 0.4 | 0.4 | 0.4 | 0.4 | 0.4 | 0.4 |
| 2^4 | 0.9 | 0.9 | 0.8 | 0.7 | 0.6 | 0.5 | 0.5 | 0.5 | 0.5 | 0.5 | 0.5 | 0.5 | 0.5 | 0.5 | 0.5 | 0.5 |
| 2^5 | 0.9 | 0.9 | 0.9 | 0.8 | 0.7 | 0.7 | 0.6 | 0.6 | 0.6 | 0.6 | 0.6 | 0.7 | 0.6 | 0.7 | 0.6 | 0.6 |
| 2^6 | 1 | 1 | 1 | 0.9 | 0.9 | 0.9 | 0.9 | 0.9 | 0.9 | 0.9 | 0.9 | 0.9 | 0.9 | 0.9 | 0.9 | 0.9 |
| 2^7 | 1 | 1 | 1 | 1 | 1 | 1.1 | 1.2 | 1.2 | 1.2 | 1.2 | 1.2 | 1.2 | 1.2 | 1.2 | 1.2 | 1.2 |
| 2^8 | 1 | 1 | 1 | 1.1 | 1.1 | 1.1 | 1.3 | 1.3 | 1.3 | 1.3 | 1.3 | 1.3 | 1.3 | 1.3 | 1.3 | 1.3 |
| 2^9 | 1.1 | 1.1 | 1.1 | 1.1 | 1.1 | 1.2 | 1.4 | 1.3 | 1.3 | 1.3 | 1.4 | 1.3 | 1.4 | 1.3 | 1.4 | 1.4 |

less numerous than pixels) makes the learning task difficult for a classifier such as RF.

3.4 Parameter Values

In all our tests, following the recommendation of Achanta et al.,⁴⁵ we used the SLIC oversegmentation algorithm with a compactness parameter equal to 10. In SaF, we group pixels into about 3000 superpixels. For the SVM, γ parameter was equal to 4 and C parameter was equal to 4. On all experimental datasets, these values provide satisfactory results, but are not critical.

4 Evaluation of SaF

4.1 State-of-the-Art Benchmarks

We compared SaF to results achieved by the height of state-of-the-art methods: three region-based interactive binarization methods (IGC,¹⁶ SIOX,¹⁷ and BPT²⁵), one boundary-based interactive binarization method (CPP),²¹ and four multiclass methods (SRG,¹⁵ IMS,²⁶ RIMSAED,²⁸ and RIIS³²). Figure 8 shows examples of segmentations produced by SaF on images of state-of-the-art benchmarks.

4.1.1 Method of Milles et al.

We compare SaF to the most recent boundary-based interactive segmentation method: CPP. This algorithm has

been evaluated by Mille et al.²¹ on a subset of 10 images, extracted from the dataset D_{MI} provided by Microsoft.⁵⁶ The accuracy of the obtained segmentations is quantified using the A_O measure of McGuinness and Oconnor²⁹

$$A_O(R, G) = 100 \frac{|G_O \cap R_O|}{|G_O \cup R_O|}, \quad (9)$$

where R_O is the set of pixels labeled as object by the algorithm, G_O is the set of pixels labeled as object in the ground truth, and $|S|$ is the cardinality of a set S . A high value of A_O indicates that the resulting regions and the regions in the ground truth are similar.

Milles et al.²¹ used automatically generated seeds: using the ground truth, the boundary of the object is extracted and split into N segments of equal length. For each segment, a seed is randomly selected. For a same image, Milles et al.²¹ computed 20 different sets of seeds. Table 5 shows the average, the standard deviation, and the maximum value of A_O scores achieved by CPP method.

Table 6 shows the performances of SaF with the same images using manually given seeds. During 2 min, the user is allowed to update seeds, improving the segmentation. The average percentage of pixels labeled as seeds by the user is equal to 0.56%.

Unfortunately, results presented in Tables 5 and 6 are not comparable. The seeds used for the evaluation of CPP are

Table 4 Error rate \mathfrak{F}_{err} (%) of SVM classifier, achieved on a subset of the ground truth of Santner et al.²⁶ The first row gives the value of C parameter, the first column gives the value of parameter γ .

| | 2^{-6} | 2^{-5} | 2^{-4} | 2^{-3} | 2^{-2} | 2^{-1} | 1 | 2 | 2^2 | 2^3 | 2^4 | 2^5 | 2^6 | 2^7 | 2^8 | 2^9 |
|----------|----------|----------|----------|----------|----------|----------|----|----|-------|-------|-------|-------|-------|-------|-------|-------|
| 2^{-6} | 22 | 22 | 22 | 22 | 21 | 18 | 15 | 13 | 12 | 11 | 10 | 10 | 9 | 8 | 8 | 6 |
| 2^{-5} | 23 | 22 | 22 | 21 | 18 | 15 | 13 | 12 | 11 | 10 | 10 | 9 | 8 | 7 | 6 | 5 |
| 2^{-4} | 22 | 22 | 21 | 18 | 15 | 13 | 12 | 11 | 10 | 9 | 8 | 7 | 6 | 5 | 5 | 4 |
| 2^{-3} | 22 | 21 | 18 | 15 | 12 | 11 | 11 | 10 | 9 | 7 | 6 | 5 | 5 | 4 | 4 | 4 |
| 2^{-2} | 21 | 18 | 15 | 13 | 11 | 10 | 9 | 8 | 7 | 6 | 5 | 4 | 4 | 4 | 3 | 3 |
| 2^{-1} | 19 | 15 | 12 | 11 | 9 | 8 | 7 | 6 | 5 | 4 | 4 | 4 | 3 | 3 | 3 | 3 |
| 1 | 16 | 12 | 10 | 9 | 7 | 6 | 5 | 4 | 4 | 3 | 3 | 3 | 3 | 3 | 3 | 3 |
| 2 | 13 | 10 | 8 | 7 | 6 | 5 | 4 | 4 | 3 | 3 | 3 | 3 | 3 | 3 | 3 | 3 |
| 2^2 | 13 | 8 | 6 | 5 | 4 | 4 | 3 | 3 | 3 | 3 | 3 | 3 | 3 | 3 | 3 | 3 |
| 2^3 | 14 | 7 | 5 | 4 | 4 | 3 | 3 | 3 | 2 | 2 | 2 | 2 | 3 | 3 | 3 | 3 |
| 2^4 | 16 | 10 | 5 | 4 | 3 | 3 | 3 | 2 | 2 | 2 | 2 | 2 | 3 | 3 | 3 | 3 |
| 2^5 | 17 | 15 | 7 | 3 | 3 | 3 | 2 | 2 | 2 | 2 | 2 | 2 | 3 | 3 | 3 | 3 |
| 2^6 | 19 | 18 | 14 | 6 | 3 | 3 | 3 | 3 | 3 | 3 | 3 | 3 | 3 | 3 | 3 | 3 |
| 2^7 | 18 | 18 | 17 | 13 | 5 | 3 | 3 | 3 | 3 | 3 | 3 | 3 | 3 | 3 | 3 | 3 |
| 2^8 | 20 | 20 | 19 | 18 | 13 | 6 | 4 | 4 | 4 | 4 | 4 | 4 | 4 | 4 | 4 | 4 |
| 2^9 | 20 | 20 | 21 | 20 | 20 | 14 | 7 | 7 | 7 | 7 | 7 | 7 | 7 | 7 | 7 | 7 |

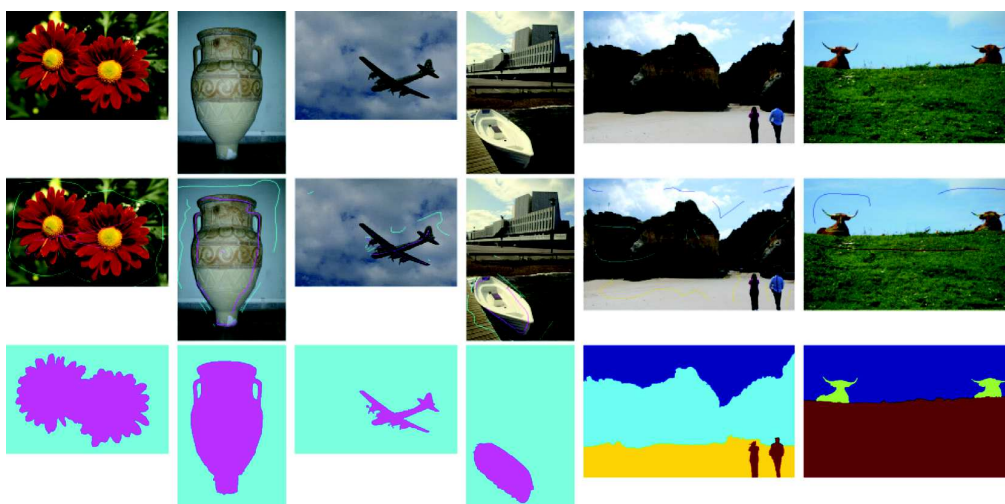


Fig. 8 Examples of segmentations produced with $S\alpha F$ on D_{MI} dataset²¹ (columns 1 and 2), D_{MG} dataset²⁹ (columns 3 and 4) and D_{SA} dataset²⁶ (columns 5 and 6). The first row shows the original image, the second row the given seeds, and the third row the result.

created using the ground truth and are more accurately located than seeds manually given by a user. In addition, seeds used for the evaluation of $S\alpha F$ are updated by the user.

With less than three iterations, $S\alpha F$ is able to achieve very satisfactory results on these datasets. In addition, $S\alpha F$ execution time does not depend on the number of seeds. Section 4.3 shows that this execution time is related to

Table 5 Performances achieved by CPP, reported from the paper of Milles et al.²¹

| Image | CPP avg | CPP std | CPP max |
|----------|---------|---------|---------|
| Banana1 | 60.4 | 0.20 | 89.1 |
| Banana2 | 47.3 | 0.25 | 88.3 |
| Banana3 | 62.5 | 0.15 | 86.6 |
| Ceramic | 85.6 | 0.03 | 89.8 |
| Doll | 80.8 | 0.04 | 87.7 |
| Flower | 88.1 | 0.29 | 98.2 |
| Mushroom | 61.3 | 0.17 | 91.1 |
| Music | 97.8 | 0.01 | 98.6 |
| Sheep | 77.0 | 0.18 | 90.2 |
| Teddy | 74.9 | 0.17 | 96.7 |
| All | 73.5 | 0.23 | 91.4 |

the number of pixels during the initialization stage and to the number of superpixels during the segmentation stages. The initialization stage can be done once, while the user is selecting the first seeds. So, only the execution time of the segmentation is perceived by the user. On the contrary, CPP execution time depends both on the image size and on the number of seeds. The average execution time for SaF is equal to 0.4 s for the initialization stage and to 0.2 s for each segmentation stage. The execution time of CPP varies between 3 and 17 s using similar hardware.

Table 6 Performances achieved by SaF.

| Image | SaF |
|----------|------|
| Banana1 | 97.1 |
| Banana2 | 96.4 |
| Banana3 | 97.9 |
| Ceramic | 97.5 |
| Doll | 98.9 |
| Flower | 98.6 |
| Mushroom | 97 |
| Music | 98.9 |
| Sheep | 96.2 |
| Teddy | 95.8 |
| All | 97.2 |

Table 7 Evaluation of SaF with McGuinness et al. protocol and comparison with IGC, SIOX, BTP, and SRG methods.²⁹

| | IGC | SIOX | BTP | SRG | SaF |
|-------|-----|------|-----|-----|-----------|
| A_O | 92 | 85 | 92 | 88 | 95 |
| A_B | 77 | 64 | 78 | 70 | 83 |

4.1.2 Methods evaluated by McGuinness et al.

The methods SRG, IGC, SIOX, and BPT have been evaluated by McGuinness et al.²⁹ on the dataset D_{MG} provided by the authors,⁵⁶ using boundary (A_B) and object (A_O) accuracy measures.²⁹ Given a segmentation result R and a ground truth G , the boundary accuracy measure is given by

$$A_B(R, G) = 100 \frac{\sum_x \min[\tilde{B}_G(x), \tilde{B}_R(x)]}{\sum_x \max[\tilde{B}_G(x), \tilde{B}_R(x)]}, \quad (10)$$

where B_G and B_R are the internal border pixels for ground truth and algorithm segmentation result, respectively, and \tilde{B}_G and \tilde{B}_R are these same sets extended using fuzzy-set theory as described in the paper of McGuinness et al.²⁹ A high value of A_B score indicates that boundaries in the segmentation result follow boundaries in the ground truth.

For each method, seeds are manually given by a user. The user has 2 min to update these seeds and achieve a segmentation as accurate as possible.

Table 7 shows that SaF outperforms these four methods with a 5% increase on A_B , a 3% increase on A_O , and a similar execution time.

4.1.3 Method of Jian et al.

We cannot make a rigorous comparison between SaF and a recent interactive binarization method based on an ACP, proposed by Jian and Jung³¹ Indeed, this paper does not contain sufficient information about the dataset used, which is an extended version of the one created by McGuinness and Oconnor.²⁹ We simply notice that SaF results on McGuinness et al. dataset²⁹ are superior to ACP scores reported by the authors, with a 1% increase. SaF execution times are slightly superior, but this drawback must be balanced by the possibility to compute the initialization stage while the user gives the seeds, to obtain a perceived SaF execution time less than or equal to ACP.

4.1.4 Methods of Santner et al. and Müller et al.

IMS and RIMSAED have been evaluated by Santner et al.²⁶ using the dataset D_{SA} ⁵⁵ provided by the authors and the DICE measure, suggested by Dice and defined in their paper. This measure is an adaptation of A_O for multiclass problems

$$DICE(R, G) = 100 \sum_{i=1}^K 2 \frac{|R_i \cap G_i|}{|R_i \cup G_i|}, \quad (11)$$

where K is the number of classes, R_i is the set of pixels of the i 'th class in the resulting segmentation, and G_i is the set of pixels of the i 'th class in the ground truth.

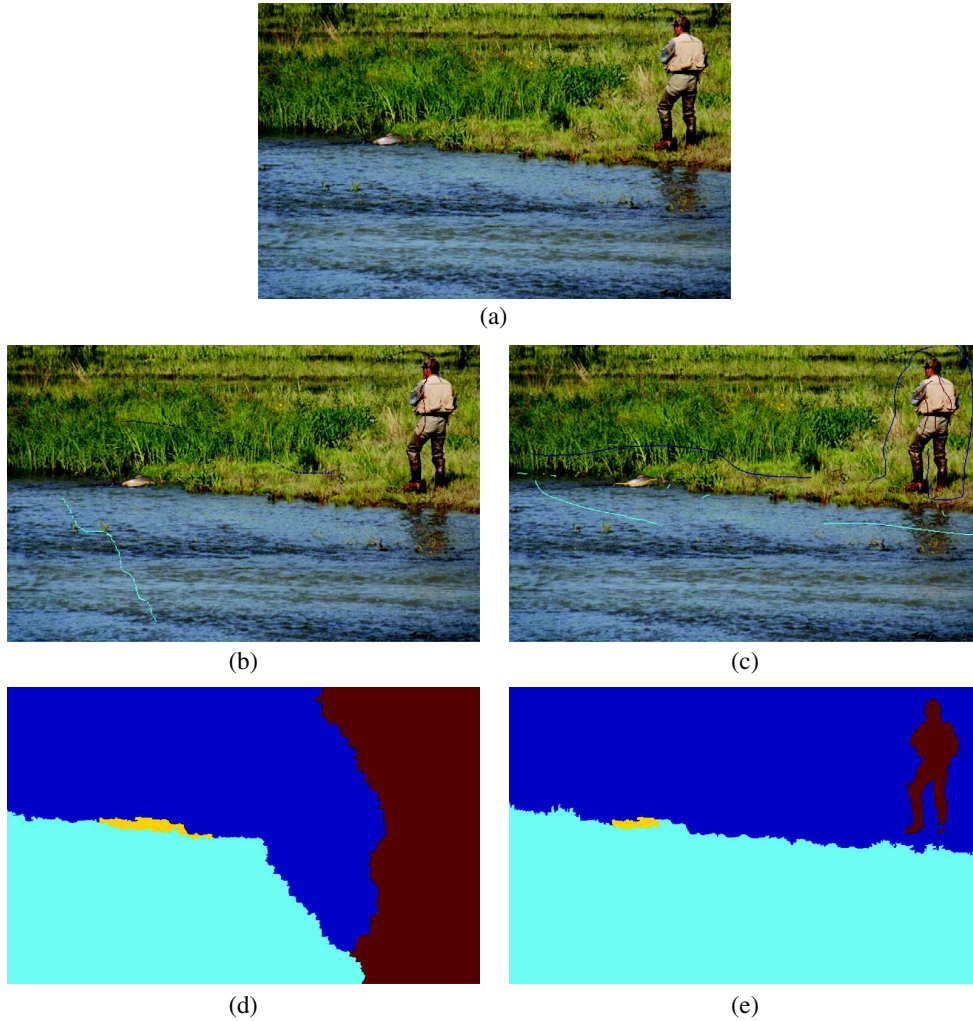


Fig. 9 Examples where seeds of Santner et al.²⁶ are inadequate in location and number for $S\alpha F$ to accurately segment the image. (a) Image 0011, (b) seeds of Santner et al., (c) seeds given by asking the user to select them near the object boundaries, (d) result with seeds of Santner et al., and (e) Result with seeds near the object boundaries.

Both Santner et al.²⁶ and Müller et al.²⁸ used the same seeds, given by the user during the creation of the ground truth. These seeds are not updated to improve the segmentation result.

With these seeds, the overall performance of $S\alpha F$ is not satisfactory, with an average DICE score of 83. The values vary between 40 and 99 and the standard deviation is around 14, indicating a high dispersion. A detailed analysis of the score distribution shows that the dataset can be divided into three groups: 32% of the images give a very good DICE score (more than 93), 35% a good DICE score (between 80 and 93), and 33% a bad DICE score (less than 80). This latter category of images explains the weak average performance of $S\alpha F$.

For these images, the provided seeds are not suitable for $S\alpha F$. Because $S\alpha F$ uses location information, it obtains unsatisfactory results when seeds are given too far from the object boundaries. Examples of such unsuitable locations are given in Figs. 9 and 10. For some images, seeds need to be located near the boundaries and more numerous (Fig. 9).

For others, modifying their locations is enough for $S\alpha F$ to get good results (Fig. 10).

To produce accurate results, $S\alpha F$ needs an instruction to be given to the user: “give the initial seeds near the object boundaries.” In the case of D_{SA} dataset, a maximum distance around 30 pixels is quite enough. As explained in Sec. 4.4, this is a small price to pay for a method showing an easily predictable behavior.

For each image, we made an additional test taking into account the instruction and allowing the user to modify the seeds in order to improve the segmentation result. We calculated the DICE score obtained with two sets of seeds: the set of initial seeds given before the first segmentation and the set of final seeds selected when the user is satisfied with the result. The average number of updates between the first segmentation and the final result is equal to 3. $S\alpha F$ produced accurate results with an average DICE score of 97 for the set of initial seeds and of 98 for the set of final seeds. The average execution time of $S\alpha F$ was only 1.2 s against 2 s for IMS and for RIMS AED. In addition, these execution

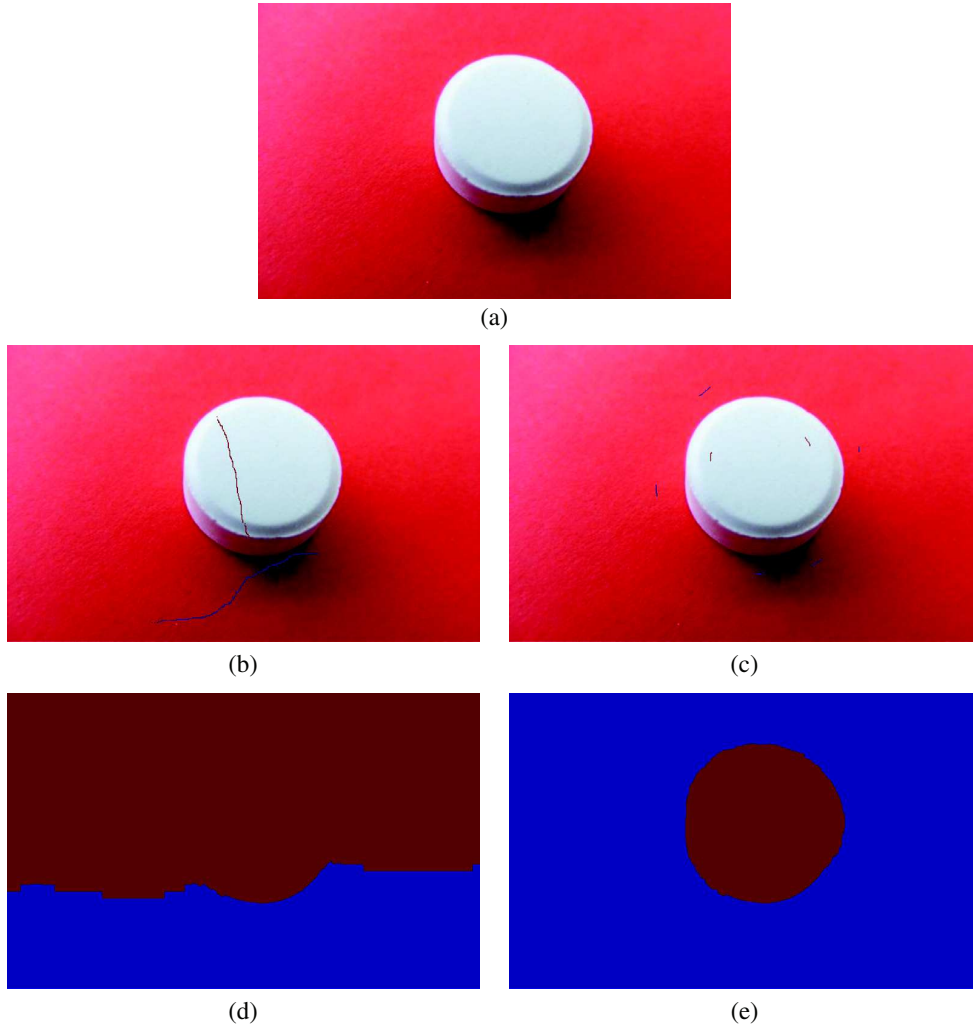


Fig. 10 Examples where seeds of Santner et al.²⁶ are inadequate in location for S α F to accurately segment the image. (a) Image 0217, (b) seeds of Santner et al., (c) seeds given by asking the user to select them near the object boundaries, (d) Result with seeds of Santner et al., and (e) Result with seeds near the object boundaries.

times, on the contrary for IMS and RIMSAED, are achieved without any specific optimization. In particular, S α F does not require a GPU implementation.

4.1.5 Method of Oh et al.

RIIS has been evaluated on D_{MI} and D_{SA} datasets, both with DICE measure, with manually given seeds. In the same conditions, S α F outperforms RIIS in terms of accuracy, with a 5% increase on D_{MI} dataset and an 8% increase on D_{SA} dataset (Table 8). The method S α F is also much more efficient with an execution time of about 1 s on a simple desktop computer, whereas RIIS running time is greater than 40 s.

4.2 Benefit of the Regularization Term

To analyze the benefit of the regularization term, we design more simple versions of S α F minimizing

$$E_{SCIS}(c|I) = \prod_{i=1}^N \mathfrak{S}^{\text{data}}(x_i, c_i). \quad (12)$$

The minimization of E_{SCIS} is easily achieved by simply keeping the classification produced by the SVM. So, we name this algorithm SCIS for superpixel classification-based interactive segmentation. We made tests on D_{MG} , D_{MI} ,²⁹ and D_{SA} dataset.²⁶ Table 9 gives the percentage of pixels used as seeds (Pr), execution time (s) for the initialization step (T_{init}), and segmentation time (s) for the segmentation step, which are required for both SCIS and S α F achieve similar accuracy. In other words, A_O and A_B scores on D_{MG} dataset,²⁹ A_O score on D_{MI} dataset,²¹ and DICE score on D_{SA} dataset²⁶ are similar.

These results show that the introduction of a regularization term in S α F reduces the required number of pixels labeled as seeds of about 1%. Concretely, SCIS uses more than 200,000 supplementary seeds. In addition, these seeds cannot be

Table 8 Comparison between RIIS and S α F on the D_{MI} and the D_{SA} datasets, with the DICE measure (%).

| | RIIS | S α F |
|-------------------------------|------|--------------|
| D_{MI} , ²¹ DICE | 93 | 98 |
| D_{SA} , ²⁶ DICE | 90 | 98 |

obtained by giving a simple instruction. Figure 11 shows an example of differences between SCIS and S α F seeds. Execution time is not significantly increased by introducing the regularization term. The initialization stage is not impacted and the segmentation stage remains about 1 s.

4.3 Scalability

We also investigate the ability of S α F to segment images of various sizes, especially images with several million pixels. As none of the previous benchmarks provides a dataset with such images, we selected 50 images from HSID and adapted them to evaluate multiclass interactive segmentation methods. We created four datasets, by rescaling these images and the ground truth: the first with big images (2,161,800 pixels), the second with medium images (1,216,350 pixels), the third with small images (684,788 pixels), and the last with tiny images (167,000 pixels).

For each dataset, we compute the mean, the standard deviation, the minimum value and the maximum value of the execution time for the initialization stage (Table 10),

Table 10 S α F initialization stage execution time in seconds.

| Size | Mean \pm std | Min | Max |
|--------|-----------------|------|------|
| Tiny | 0.47 \pm 0.08 | 0.42 | 1.03 |
| Small | 1.79 \pm 0.06 | 1.71 | 1.98 |
| Medium | 3.25 \pm 0.12 | 3.06 | 3.64 |
| Big | 5.73 \pm 0.25 | 5.34 | 6.33 |

the execution time for the segmentation stage (Table 11) and the DICE measure (Table 12).

The low standard deviation and the small difference between maximum and minimum values shows that the quality of S α F results and the time required are not strongly altered by the number of classes. The most interesting conclusion on this experimentation is the gap between the execution time for the initialization stage and the execution time for the segmentation stage. As initialization must be done only once, this stage has little impact on S α F responsiveness. In fact, with an implementation performing this stage while the user gives seeds, S α F can become an interactive time application, computing the segmentation stage in less than 1 s, even for images with millions of pixels. In addition, because the superpixel number is always around 3000, the execution time for the segmentation stage is stable, even if the image size is significantly increased. The DICE score shows that this ‘‘compression’’ of the image is sufficient to ensure accurate results, no matter the image size.

Table 9 Comparison of the required percentage of pixels labeled as seeds (Pr), execution time in seconds for the initialization step (T_{init}) and segmentation time in seconds for the segmentation step (T_{seg}) for both SCIS and S α F. The three scores are obtained for segmentations of similar accuracy.

| Bench. | D_{MG} ²⁹ | | D_{MI} ²¹ | | D_{SA} ²⁶ | |
|----------------|------------------------|-----------------|------------------------|-----------------|------------------------|-----------------|
| | SCIS | S α F | SCIS | S α F | SCIS | S α F |
| Pr (%) | 2.08 \pm 0.49 | 1.26 \pm 0.69 | 2.08 \pm 0.49 | 0.74 \pm 0.36 | 1.42 \pm 0.42 | 0.89 \pm 0.43 |
| T_{init} (s) | 0.4 \pm 0.01 | 0.41 \pm 0.01 | 0.6 \pm 0.18 | 0.61 \pm 0.19 | 0.64 \pm 0.02 | 0.66 \pm 0.02 |
| T_{seg} (s) | 0.06 \pm 0.03 | 0.68 \pm 0.04 | 0.04 \pm 0.02 | 0.27 \pm 0.02 | 0.06 \pm 0.04 | 0.51 \pm 0.28 |

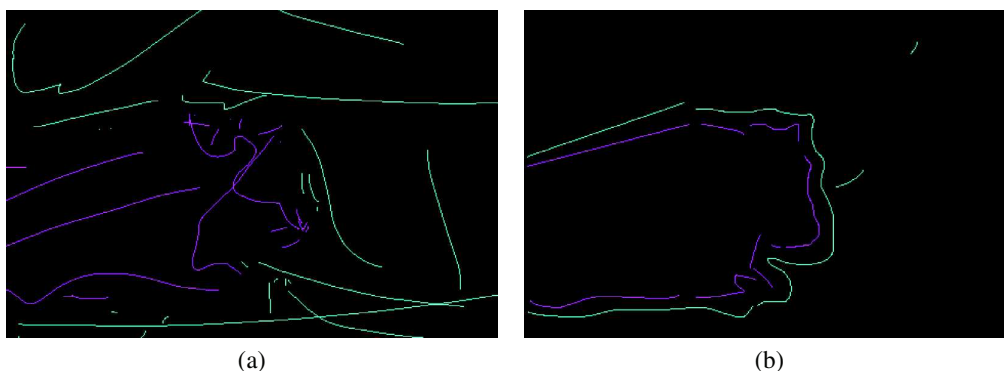


Fig. 11 Comparison between (a) SCIS and (b) S α F seeds.

Table 11 S α F segmentation stage execution time in seconds.

| Size | Mean \pm std | Min | Max |
|--------|-----------------|------|------|
| Tiny | 0.49 \pm 0.27 | 0.23 | 1.69 |
| Small | 0.46 \pm 0.28 | 0.21 | 1.64 |
| Medium | 0.46 \pm 0.28 | 0.21 | 1.68 |
| Big | 0.41 \pm 0.22 | 0.2 | 1.2 |

Table 12 S α F DICE score.

| Size | Mean \pm std | Min (%) | Max (%) |
|--------|----------------|---------|---------|
| Tiny | 98% \pm 4.72 | 66 | 100 |
| Small | 99% \pm 1.03 | 95 | 100 |
| Medium | 99% \pm 0.99 | 95 | 100 |
| Big | 99% \pm 1.12 | 95 | 100 |

4.4 Usability

4.4.1 Time required to segment an image

A fully manual segmentation of an image is a time-consuming task. To create the reference segmentations of HSID, we spent around 1 h per image to achieve a level of accuracy high enough to meet the requirements of a ground truth

data. However, we are comfortable with graphic tablets. Beginners need more time to get an accurate segmentation.

Using S α F significantly facilitates and accelerates the segmentation process. The overall time to segment an image—including the selection of initial seeds, the corrections of seeds and the execution time of each use of S α F—is related:

- to the number of classes: several classes require more seeds and to often change the color of the brush-like tool used to select them;
- to the image complexity: if an object contains a lot of small and scattered details, selection of seeds is more difficult.

With McGuinness et al.,²⁹ in the worst case, the overall time is 2 min. In the best case, only a few seconds are required to segment an image. With Santner et al.,²⁶ in the worst case, this duration is around 5 min. In the best case, only a few seconds are required to segment an image. The selection of the initial seeds is the more time-consuming task. The computation time of each run of the segmentation stage of S α F is lower than 1 s. The correction of seeds takes only a few seconds.

Table 13 shows three examples of time needed for fully manually segmenting an image versus using S α F. The first image (Fig. 12) is a small image of the McGuinness et al. dataset,²⁹ whereas the last two images (Figs. 13 and 14) come from the HSID dataset. The overall segmentation time using S α F is detailed into the last four columns of this table. On these images, using S α F is 6 to 11 times faster than a fully manual segmentation.

Table 13 Examples of time needed for a user to perform a fully manual segmentation of an image versus using S α F (s).

| Image | Fully manual | Using S α F | | | | |
|---------|--------------|--------------------|------------------------|------------------|----------------------|--------------------|
| | | Overall time | Initial seed selection | Seed corrections | Initialization stage | Segmentation stage |
| Fig. 12 | 216 | 34 | 27 | 5 | 0.5 | 1.5 |
| Fig. 13 | 634 | 37.5 | 25 | 6 | 5.5 | 1 |
| Fig. 14 | 893 | 76.5 | 62 | 8 | 5.5 | 1 |

**Fig. 12** S α F seed evolution example for a binarization problem. Only two updates of seeds are required to achieve an accurate result.

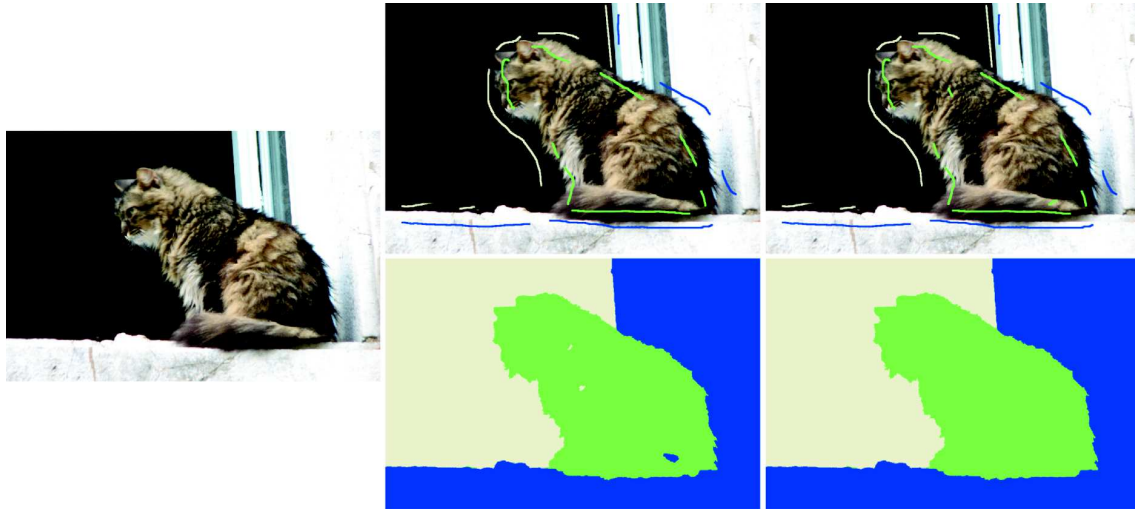


Fig. 13 SaF seed evolution example for a problem with three classes. Only one update of seeds is required to achieve an accurate result.

In the case of Fig. 12, where a church must be extracted and where the foreground is clearly separate from the background, only a few seeds are necessary. The user who segmented this image was familiar with SaF: drawing some strokes to obtain the first segmentation result took only a few seconds. Additional tests show us that less experienced users need more time (several tens of seconds) for the first image because they select more seeds, following more scrupulously the object boundaries. Fortunately, they learn quickly how to reduce the number of seeds. The correction of errors in the result given by SaF by adding or removing seeds is straightforward: for both novice and expert users, each correction takes less than 1 s.

4.4.2 Predictability

The user evaluation results of the McGuinness et al. review²⁹ highlight the necessity for an interactive segmentation method to not only provide a fast and accurate segmentation, but also to have a predictable behavior.

Figures 12–14 show examples of segmentations achieved with SaF for images taken from datasets used in Secs. 4.1

and 4.3. The analysis of the given seeds shows that the behavior of SaF is easily predictable: by putting seeds near the objects borders, the majority of the image is correctly segmented. In the majority of the cases, the remaining errors are quickly corrected by adding seeds over them. If some errors are due to seeds put on the wrong object, these seeds can be removed. This good predictability is directly related to the choice of the superpixel features: as color and location are extremely intuitive concepts, the behavior of SaF is consistent with the user expectation.

Moreover, for the images of Figs. 12–14, a maximum of two updates of the seeds allow achieving a correct segmentation. Except for particularly difficult situations with, for example, shadows or a poor contrast between objects, the required number of iterations varies from 2 to 4. If seeds are correctly positioned with respect the object boundaries, only small errors have to be corrected and the accuracy of the segmentation at each iteration is not strongly improved. For example, on the dataset of Santner et al.,²⁶ between the initial and the final segmentations, the average DICE score has improved from about 97 to 98. This fast convergence and



Fig. 14 SaF seed evolution example for a problem with four classes. Only two updates of seeds are required to achieve an accurate result.

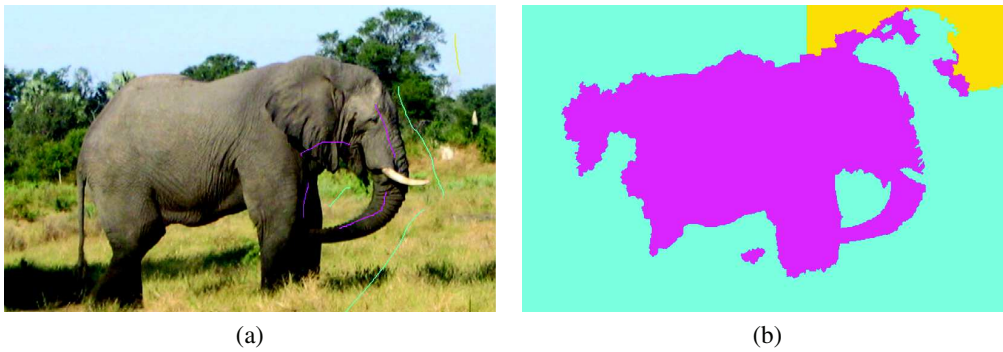


Fig. 15 $S\alpha F$ failing to produce an accurate segmentation when user gives wrong seeds. (a) $S\alpha F$ seeds and (b) segmentation result.

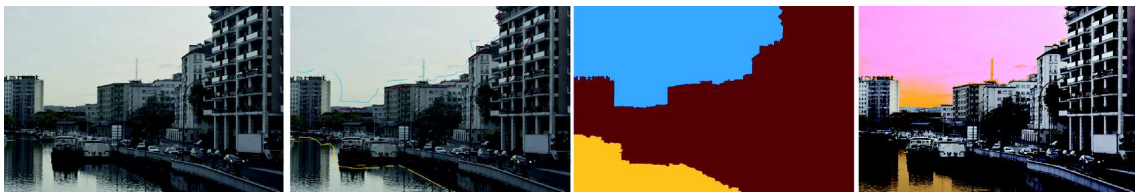


Fig. 16 Usage of $S\alpha F$ for photo enhancement. From the left to the right: original image, seeds, segmentation result, and enhanced photograph.

the fact that only some strokes are required to segment an image make us confident about the user acceptance of $S\alpha F$ as a tool for multiple object selection.

However, when first seeds are not given near the boundary, $S\alpha F$ can produce segments with significant errors. Notably, if the seeds are given only on a small part of the image, superpixels used as training data can be insufficient to find the right support vector during SVM training. An example is given in Fig. 15. Fortunately, these errors are easily avoided by asking the user to give seeds near the boundaries.

5 Applications

5.1 Semantic Segmentation for Landscape Observatories

Since 2005, the European Landscape Convention of the Council of Europe⁵⁷ promotes the protection and management of European landscapes. In this context, landscape observatories^{58–60} respond to the need to study the landscape and build awareness of society to their conservation. They are based on digital photograph datasets, containing for several interesting spots a chronological series of photographs, taken regularly (for example, every month or every year).

The algorithm $S\alpha F$ has been implemented in an Android application allowing to update the images of a landscape observatory and to segment them into labeled regions, related to landscape semantic elements (building, grass, road, etc.). The application locates the nearest observatory spot and downloads a previous photograph of the spot to easily re-photograph it. Then, it uses $S\alpha F$ to produce semantic segmentation of the photograph, which allows a quick automatic comparison of images of the same spot to detect interesting changes. The complete framework has been presented during the 2017 French Conference on Multimedia, Geomatics,

Teaching, and Learning⁶¹ and will be used very soon with school students in life and agronomy sciences and technologies and landscape design.

5.2 Photograph Enhancement

Figure 16 shows an example of $S\alpha F$ usage to enhance a photograph using Gimp. Thanks to $S\alpha F$, three different image regions are selected, corresponding to the sky, the building, and the water. Notice that the original image is especially difficult with a poor contrast between the water and the buildings, dull colors, and thin elements. Then, we applied to each region a specific operator to enhance it and modified the color channels of the sky to create a sunset feeling; we increased the contrast and the color saturation of the buildings and made the water darker with golden light reflections. Each local modification allows a more visually pleasant global image.

6 Conclusions

In this paper, we proposed an interactive multiclass segmentation method, $S\alpha F$. This algorithm is based on the modeling of the interactive segmentation problem as a factor graph, where variables are superpixels and factors allow to minimize both a data term and a regularization term. By comparing $S\alpha F$ with the state-of-the-art algorithms on current benchmarks, we show that it is a very competitive algorithm. We also provide extended tests, allowing to better understand the influence of each component of the proposed method. In particular, we made available a dataset for oversegmentation methods evaluation, providing results missed by the previous reviews about superpixel algorithms. In addition, we made available three datasets to check scalability of interactive segmentation methods and show that $S\alpha F$ successfully segments them.

The performance achieved by SaF on the six tested datasets shows the ability of superpixels to provide an efficient compression of the image. The execution time of SaF highlights their relevance to design competitive computer vision algorithms. Here, they are the key to provide a scalable method producing a result in interactive time.

We also described SaF usage in two different applications: photograph enhancement and semantic segmentation.

The source code of SaF, the three datasets used for the scalability evaluation, and the seeds are made available at Ref. 56.

Acknowledgments

The work of Bérengère Mathieu was partially supported by ANR-11-LABX-0040-CIMI within the program ANR-11-IDEX-0002-02.

References

- J. Long, E. Shelhamer, and T. Darrell, "Fully convolutional networks for semantic segmentation," in *IEEE Conf. on Computer Vision and Pattern Recognition*, pp. 3431–3440 (2015).
- A. Garcia-Garcia et al., "A review on deep learning techniques applied to semantic segmentation," *Comput. Res. Repository* abs/1704.06857 (2017).
- D. Fourure et al., "Multi-task, multi-domain learning: application to semantic segmentation and pose regression," *Neurocomputing* **251**, 68–80 (2017).
- D. Lin et al., "ScribbleSup: scribble-supervised convolutional networks for semantic segmentation," in *IEEE Conf. on Computer Vision and Pattern Recognition*, pp. 3159–3167 (2016).
- N. Ben-Zadok, T. Riklin-Raviv, and N. Kiryati, "Interactive level set segmentation for image-guided therapy," in *IEEE Int. Symp. on Biomedical Imaging: From Nano to Macro*, pp. 1079–1082 (2009).
- D. Cremers et al., "A probabilistic level set formulation for interactive organ segmentation," *Proc. SPIE* **6512**, 65120V (2007).
- A. X. Falcão, J. K. Udupa, and F. K. Miyazawa, "An ultra-fast user-steered image segmentation paradigm: live wire on the fly," *IEEE Trans. Med. Imaging* **19**(1), 55–62 (2000).
- Y. Gao et al., "A 3D interactive multi-object segmentation tool using local robust statistics driven active contours," *Med. Image Anal.* **16**(6), 1216–1227 (2012).
- Y. Tong et al., "Interactive iterative relative fuzzy connectedness lung segmentation on thoracic 4D dynamic MR images," *Proc. SPIE* **10137**, 1013723 (2017).
- J. Egger et al., "US-cut: interactive algorithm for rapid detection and segmentation of liver tumors in ultrasound acquisitions," *Proc. SPIE* **9790**, 97901C (2016).
- H.-E. Gueziri, M. J. McGuffin, and C. Laporte, "A generalized graph reduction framework for interactive segmentation of large images," *Comput. Vision Image Understanding* **150**, 44–57 (2016).
- T. Suzuki et al., "Interactive segmentation of pancreases from abdominal CT images by use of the graph cut technique with probabilistic atlases," in *Int. Conf. on Innovation in Medicine and Healthcare*, pp. 575–584, Springer (2015).
- P. Karasev et al., "Interactive medical image segmentation using PDE control of active contours," *IEEE Trans. Med. Imaging* **32**, 2127–2139 (2013).
- J. Petersena et al., "Effective user guidance in online interactive semantic segmentation," *Proc. SPIE* **10134**, 101341V (2017).
- R. Adams and L. Bischof, "Seeded region growing," *IEEE Trans. Pattern Anal. Mach. Intell.* **16**(6), 641–647 (1994).
- Y. Boykov and M.-P. Jolly, "Interactive graph cuts for optimal boundary and region segmentation of objects in ND images," in *IEEE Int. Conf. on Computer Vision*, Vol. 1, pp. 105–112 (2001).
- G. Friedland, K. Jantz, and R. Rojas, "SIOX: simple interactive object extraction in still images," in *IEEE Int. Symp. on Multimedia* (2005).
- L. Grady, "Random walks for image segmentation," *IEEE Trans. Pattern Anal. Mach. Intell.* **28**(11), 1768–1783 (2006).
- V. Gulshan et al., "Geodesic star convexity for interactive image segmentation," in *IEEE Computer Society Conf. on Computer Vision and Pattern Recognition*, pp. 3129–3136 (2010).
- Y. Li et al., "Lazy snapping," *ACM Trans. Graphics* **23**(3), 303–308 (2004).
- J. Mille, S. Bougleux, and L. D. Cohen, "Combination of piecewise-geodesic paths for interactive segmentation," *Int. J. Comput. Vision* **112**(1), 1–22 (2015).
- P. A. Miranda, A. X. Falcao, and T. V. Spina, "Riverbed: a novel user-steered image segmentation method based on optimum boundary tracking," *IEEE Trans. Image Process.* **21**(6), 3042–3052 (2012).
- E. N. Mortensen and W. A. Barrett, "Interactive segmentation with intelligent scissors," *Graphical Models Image Process.* **60**(5), 349–384 (1998).
- J. Ning et al., "Interactive image segmentation by maximal similarity based region merging," *Pattern Recognit.* **43**(2), 445–456 (2010).
- P. Salembier and L. Garrido, "Binary partition tree as an efficient representation for image processing, segmentation, and information retrieval," *IEEE Trans. Image Process.* **9**(4), 561–576 (2000).
- J. Santner, T. Pock, and H. Bischof, "Interactive multi-label segmentation," in *Asian Conf. on Computer Vision*, pp. 397–410 (2010).
- A. Blake et al., "Interactive image segmentation using an adaptive GMMRF model," in *European Conf. on Computer Vision*, pp. 428–441 (2004).
- S. Müller et al., "Robust interactive multi-label segmentation with an advanced edge detector," in *German Conf. on Pattern Recognition*, pp. 117–128 (2016).
- K. McGuinness and N. E. Oconnor, "A comparative evaluation of interactive segmentation algorithms," *Pattern Recognit.* **43**(2), 434–444 (2010).
- Y. Rubner, C. Tomasi, and L. J. Guibas, "The earth mover's distance as a metric for image retrieval," *Int. J. Comput. Vision* **40**(2), 99–121 (2000).
- M. Jian and C. Jung, "Interactive image segmentation using adaptive constraint propagation," *IEEE Trans. Image Process.* **25**(3), 1301–1311 (2016).
- C. Oh, B. Ham, and K. Sohn, "Robust interactive image segmentation using structure-aware labeling," *Expert Syst. Appl.* **79**, 90–100 (2017).
- P. Dollár and C. L. Zitnick, "Fast edge detection using structured forests," *IEEE Trans. Pattern Anal. Mach. Intell.* **37**(8), 1558–1570 (2015).
- C. Nieuwenhuis and D. Cremers, "Spatially varying color distributions for interactive multilabel segmentation," *IEEE Trans. Pattern Anal. Mach. Intell.* **35**(5), 1234–1247 (2013).
- D. Krishnan, R. Fattal, and R. Szeliski, "Efficient preconditioning of Laplacian matrices for computer graphics," *ACM Trans. Graphics* **32**(4), 142 (2013).
- J. Kappes et al., "A comparative study of modern inference techniques for discrete energy minimization problems," in *IEEE Conf. on Computer Vision and Pattern Recognition*, pp. 1328–1335 (2013).
- D. Stutz, "Superpixel segmentation: an evaluation," in *German Conf. on Pattern Recognition*, pp. 555–562 (2015).
- D. Koller and N. Friedman, *Probabilistic Graphical Models: Principles and Techniques*, MIT Press, Cambridge (2009).
- T.-F. Wu, C.-J. Lin, and R. C. Weng, "Probability estimates for multi-class classification by pairwise coupling," *J. Mach. Learn. Res.* **5**, 975–1005 (2004).
- Y. Boykov, O. Veksler, and R. Zabih, "Fast approximate energy minimization via graph cuts," *IEEE Trans. Pattern Anal. Mach. Intell.* **23**(11), 1222–1239 (2001).
- A. Fix et al., "A graph cut algorithm for higher-order Markov random fields," in *IEEE Int. Conf. on Computer Vision*, pp. 1020–1027 (2011).
- P. F. Felzenszwalb and D. P. Huttenlocher, "Efficient graph-based image segmentation," *Int. J. Comput. Vision* **59**(2), 167–181 (2004).
- A. Vedaldi and S. Soatto, "Quick shift and kernel methods for mode seeking," in *European Conf. on Computer Vision*, pp. 705–718 (2008).
- M.-Y. Liu et al., "Entropy rate superpixel segmentation," in *IEEE Conf. on Computer Vision and Pattern Recognition*, pp. 2097–2104 (2011).
- R. Achanta et al., "SLIC superpixels compared to state-of-the-art superpixel methods," *IEEE Trans. Pattern Anal. Mach. Intell.* **34**(11), 2274–2282 (2012).
- C. Conrad, M. Mertz, and R. Mester, "Contour-relaxed superpixels," in *Int. Workshop on Energy Minimization Methods in Computer Vision and Pattern Recognition*, pp. 280–293 (2013).
- A. Rubio et al., "BASS: boundary-aware superpixel segmentation," in *Int. Conf. on Pattern Recognition* (2016).
- V. Machairas et al., "Waterpixels," *IEEE Trans. Image Process.* **24**(11), 3707–3716 (2015).
- B. Mathieu, A. Crouzil, and J. B. Puel, "Heterogeneous size image dataset," image.ensfea.fr/hsid/ (2017).
- B. Mathieu, A. Crouzil, and J. B. Puel, "Oversegmentation methods: a new evaluation," in *Iberian Conf. on Pattern Recognition and Image Analysis* (2017).
- S. Gould et al., "Multi-class segmentation with relative location prior," *Int. J. Comput. Vision* **80**(3), 300–316 (2008).
- O. Barkan et al., "Fast high dimensional vector multiplication face recognition," in *IEEE Int. Conf. on Computer Vision*, pp. 1960–1967 (2013).
- S. Bochkhanov, "ALGLIB®—numerical analysis library," www.alglib.net (1999).
- C. C. Chang and C. J. Lin, "LIBSVM: a library for support vector machines," *ACM Transactions on Intelligent Systems and Technology (TIST)* **2**(3), 1–27 <http://www.csie.ntu.edu.tw/~cjlin/libsvm> (2011).
- J. Santner, "Interactive segmentation (IcgBench) dataset," gpu4vision.icg.tugraz.at/index.php?content=downloads.php (2010).

56. B. Mathieu, A. Crouzil, and J. B. Puel, "Superpixel alpha fusion: source code and datasets," image.ensfea.fr/saf/ (2017).
57. M. Déjeant-Pons, "Presentation of the European Landscape Convention of the Council of Europe," rm.coe.int/16802f7dfd (2017).
58. Landscape Observatory Consortium, "The Landscape Observatory of Catalonia," www.catpaisatge.net/eng/observatori.php (2005).
59. Fédération Inter-Environnement Wallonie, "Observatoire citoyen du paysage (in French)," www.paysages-citoyens.be/spip.php?rubrique15 (2009).
60. D. Quesney and D. Betzinger, "Observatoire des Paysages (in French)," observatoiredespaysages.fr/observatoires/ (2013).
61. J. B. Puel, B. Mathieu, and A. Crouzil, "Une application distribuée pour l'enseignement du paysage," in *Journées Géomatique, Enseignement et Apprentissage (in French)*, pp. 1960–1967 (2017).

Bérengère Mathieu received her MS degree in computer science from Paul Sabatier University, Toulouse, France, in 2012. She is currently working toward her PhD at the Institut de Recherche en Informatique de Toulouse (IRIT) Laboratory at the University of

Toulouse. Her research interests include interactive segmentation and oversegmentation.

Alain Crouzil received his PhD in computer science from Paul Sabatier University, Toulouse, France, in 1997. He is currently an associate professor at Paul Sabatier University and a member of the Traitement et Compréhension d'Images (TCI) Group of IRIT. His research interests concern stereo vision, shape from shading, camera calibration, image segmentation, change detection, and motion analysis.

Jean-Baptiste Puel received his PhD in computer science from Paul Sabatier University, Toulouse, France, in 1997. He is currently an associate professor at ENSFEA and a member of the TCI Group of IRIT. His research topics include computer vision (image segmentation and change detection) applied to the field of environmental geography (multimedia landscape observatories).